# FIRST PRINCIPLES APPROACH TO UNDERSTANDING STABILITY AND PHASE TRANSITIONS OF METAL A(II)B(IV)HEXAFLUORIDES

A Thesis
Presented to
The Academic Faculty

by

Charles A. Pueschel

In Partial Fulfillment
of the Requirements for the Degree
Master of Science in the
School of Chemical and Biomolecular Engineering

Georgia Institute of Technology
December 2015

# FIRST PRINCIPLES APPROACH TO UNDERSTANDING STABILITY AND PHASE TRANSITIONS OF METAL A(II)B(IV)HEXAFLUORIDES

Approved by:

Professor David S. Sholl, Advisor
School of Chemical and Biomolecular Engineering
*Georgia Institute of Technology*

Professor Angus P. Wilkinson
School of Chemistry and Biochemistry
*Georgia Institute of Technology*

Professor Martin Maldovan
School of Chemical and Biomolecular Engineering
*Georgia Institute of Technology*

Date Approved: 2 October 2015

# ACKNOWLEDGEMENTS

I would like to express my thanks to my advisory committee: Dr. David S. Sholl, Dr. Angus P. Wilkinson, and Dr. Martin Maldovan. I would also like to extend my thanks to the Sholl Group. In particular, Dr. David S. Sholl and Josh D. Howe for their mentoring of computational techniques without which this research would not be possible. A special thanks to Hakan Demir for getting me started with some simple phonon calculations. I would also like to thank Rebecca Han for proof reading and editing.

# TABLE OF CONTENTS

# LIST OF TABLES

# LIST OF FIGURES

# SUMMARY

Understanding the mechanisms of thermal expansion is critical for manipulating thermal behavior of new compounds. This work analyzes and predicts $A^{II}B^{IV}F_6$-type metal fluorides with interesting thermal properties. Computational modeling methods serve as a complementary method to guide experimental synthesis. The stability and thermal expansion of thirteen materials was evaluated using density functional theory methods that included vibrational density of state calculations, quasi-harmonic approximation, derived thermodynamic quantities, and phase stability analysis.

Of the thirteen materials evaluated, there were three ($CaZr_6$,$CaHfF_6$, and $MgNbF_6$) identified as being stable and demonstrating negative thermal expansion over low temperatures. The volumetric thermal expansions for $CaZr_6$,$CaHfF_6$, and $MgNbF_6$ were found to be $\alpha_{100K}$ = -2.177×$10^{-5}$, -2.17×$10^{-5}$, and -1.091×$10^{-5}$ $K^{-1}$ respectively. The phase transitions due to pressure increases were also explored for materials identified to display negative thermal expansion at low temperatures. Pressure induced phase transitions were predicted to occur at pressures beyond 475 MPa, 466 MPa, and 526.9 MPa for $CaZrF_6$, $CaHfF_6$, and $MgNbF_6$ respectively.

# CHAPTER I

# INTRODUCTION

## *1.1 Outline*

Understanding the mechanisms of thermal expansion is critical for manipulating thermal behavior of new compounds. This work analyzes and predicts $A^{II}B^{IV}F_6$-type metal fluorides with interesting thermal properties. Computational modeling methods serve as a complementary method to guide experimental synthesis.

## *1.2 Thermal Expansion in Materials*

The coefficient of thermal expansion (CTE) relates the change in volume of a material to the change in temperature:

$$\alpha_V = \frac{1}{V}\frac{\partial V}{\partial T} \tag{1}$$

A negative value for CTE indicates a contraction or negative thermal expansion (NTE) while a positive value indicates a positive thermal expansion (PTE). Although many commonly-encountered materials exhibit PTE (as shown in Table 1), the most notable exception is water. As water transitions from the liquid to ice, it expands – an increase in volume over decreasing temperature gives rise to a negative CTE, and therefore negative thermal expansion. Some less ubiquitous materials that undergo negative thermal expansions are MOFs [5][6], zeolites[7], $NaZr_2P_3O_{12}$ family[8] [9] [10] ($ZrW_2O_8$, $AM_2O_7$ (A = Ti, Zr, Hf; M = P, V), $Sc_2(WO_4)_3$[10], $Ag_3[Co(CN)_6]$[11], and $ScF_3$[12]. There is great interest in identifying candidates with NTE because they can be combined with PTE materials to create composites that have net zero thermal expansion (ZTE). Shape and volume invariance to temperature change is very desirable for obvious reasons of mechanical stability.

**Table 1:** Coefficient of Linear Thermal Expansion of Materials.

| Material | $T(^{\circ}\mathrm{C})$ | CTE ($\times 10^{-6}\ K^{-1}$) |
|---|---|---|
| Pure Antimony† | 21-100 | 8.4-11 |
| Pure Beryllium† | 21-100 | 11-12 |
| Pure Iron† | 21-100 | 12-13 |
| Platinum† | 21-100 | 8.8-9.1 |
| Pure Silver† | 21-100 | 19 |
| YbGaGe[13] | -173.2-126.9 | 0.0 |
| Zinc aluminum† | 21-100 | 22-28 |

† values are taken from [14]

### 1.2.1 Applications

The materials industries are always seeking new ways to tailor thermal expansion of new compounds. Many applications already exploit NTE or ZTE properties. One recent design for a liquefied natural gas pipeline implemented a composite with ZTE [15]. ZTE composites are also often used in precision optical mirrors that must not change with temperature. Other applications for controlled thermal expansion includes fibre optic systems, pyrex glass[16], ceramic catalysts[17], solid-oxide fuel cell[18], microelectronics[19], and thermoelectric generators[20]. Failure to correctly adjust for natural thermal expansion in these applications can result in temperature related stress failures.

### 1.2.2 Controlling NTE

The thermal expansion of a material is mainly controlled in four ways: (1) chemical substitutions, (2) particle size effects, and (3) pressure and strain from the external environment, (4) defects. In this thesis, the main focus will be on the first, however it important to understand what other effects control the thermal expansion of materials.

(1) NTE can be controlled through the substitution of atoms. In 2013, Chen *et al.*

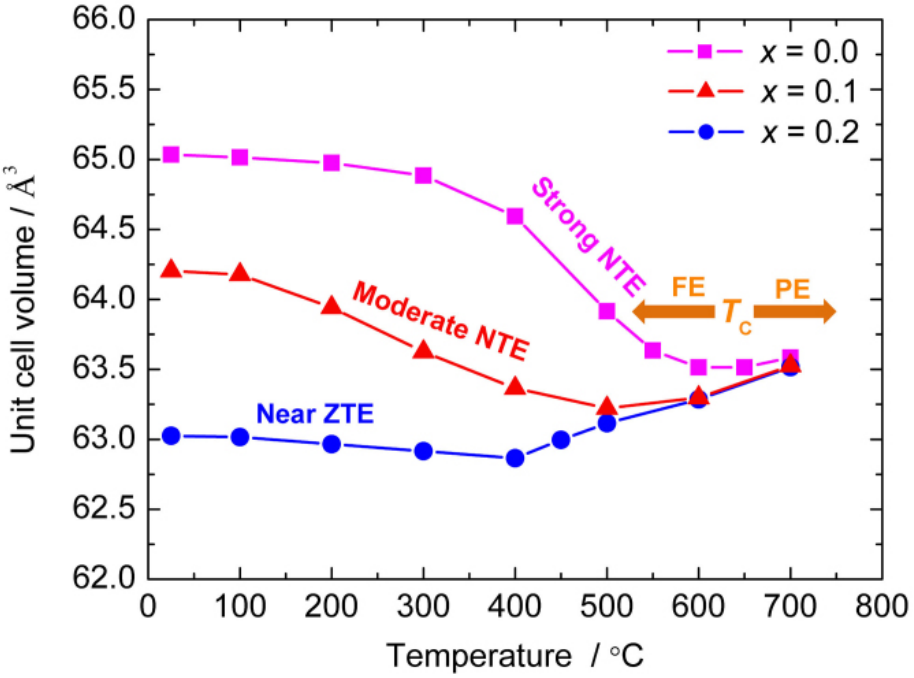


**Figure 1:** Chemical Substitution. Unit cell volume change with respect to temperature for $0.5PbTiO_3$-$0.5(Bi_{1-X}La_X)FeO_3$. Figure reproduced from [2].

demonstrated that $0.5PbTiO_3$-$0.5(Bi_{1-X}La_X)FeO_3$ could be controlled through variations in X (Figure 1). Varying the ratio of bismuth to lanthanum (X = 0, 0.1, and 0.2) produced structures with "Near ZTE", "Moderate NTE", and "Strong NTE", respectively[2].

(2) Particle size effects often impact thermal expansion properties as well. Grain boundaries along different crystal faces will have different expansion coefficients, creating interesting anisotropic thermomaterials[21].

(3) Another design parameter for systems which utilize thermal expansion to minimize stress is control of environmental pressure and strain. Many materials that exhibit variance in thermal expansion with temperature are also dependent on pressure strain effects. A system could be designed that takes advantage of these effects to create advantageous properties in thin films when put under pressure, undergo a transition, and NTE. $ZrW_2O_8$, for example, displays strong NTE effects over 0.3 to 1050 K but under a compression of 0.2 GPa a pressure induced phase transition

occurs decreasing the NTE by an order of magnitude approaching ZTE [22].
(4) Finally, defects also have a significant impact on thermal expansion, as demonstrated and theoretically explained for vacancies in metallic compounds[23].

Thermal expansion characteristics should be studied for any material of industrial application, from thin film microelectronics to advanced nanomaterials.

Different methods are more compatible with different materials, depending on the intended application. For example, thin film microelectronics are an area where precise tuning of the thermal expansion coefficient is necessary, but any defect doping or grain boundaries cannot interfere with the required purity/crystallinity of the devices. These tunable material attributes are often also correlated to other properties such as ferroelectricity, magnetism, electron configuration. [24].

## *1.3 Metal Fluoride Background*

Metal fluorides are compounds formed when fluorine (F) reacts with metal (M) to form an ionic or covalent bond, as seen in Equation 2, where n is usually anywhere from one to six fluorine atoms, and very rarely seven or eight.

$$2M + nF_2 \longrightarrow 2MF_n \tag{2}$$

Among more highly coordinated metal fluorides, variations in bonding can give rise to a variety of crystal structures with distinct electronic and vibrational states, which greatly change the material properties [25]. More complex combinations can be formed through solid-state reactions of the constituents (Equation 3). For the $A^{II}B^{IV}F_6$ type metals fluorides of interest in this research, the reaction occurs between fluoride coordinated metal cations with the addition of heat.

$$M^{(II)}F_2 + M^{(IV)}F_4 \xrightarrow{Heat} M^{(II)}M^{(IV)}F_6 \tag{3}$$

### 1.3.1 Thermal Behavior (Rigid Unit Modes)

In 2010, scientists at Georgia Tech demonstrated negative thermal expansion (NTE) in scandium trifluoride ($ScF_3$) [4]. This behavior can be explained by understanding how the thermal motions of a lattice (whether a traditional crystal, or an open-framework structure like a MOF) give rise to phonon modes. In a crystal lattice, each atom has an individual oscillation with have 3 normal modes of vibration. The linear combination of all the atomic vibrations will give rise to characteristic frequencies of the lattice, also known as phonon modes.

In systems with certain symmetry, groups of atoms that are subsets of the lattice have additional vibrational modes. An important example of this are the $ReO_3$-type materials ($A^{II}B^{IV}F_6$ metal fluorides are a member of this family) which have a cubic space group. $ReO_3$-type materials have a metal center coordinated to 6 oxygens. These coordinated metals form rigid polyhedra with oxygens at each of the vertices. The polyhedra are considered "rigid" since atoms within the polyhedral vibrate together. Adjacent polyhedra do not have to vibrate together, but can instead sustain a transverse vibration with respect to one another about the M-O-M linkages[26]. This model (see Figures 2 and 3) is known as the rigid unit mode (RUM).

Typical models approximate vibrational energies between atoms as quadratic like the characteristic harmonic spring potential and neglect higher order energies (cubic, quartic, etc.) contributions. However, in $ScF_3$, the quartic oscillations at lower temperatures have been shown to be comparable to its quadratic frequencies with rigid unit modes (RUMs) present [27]. By performing simulations[1] of the structure's atomic vibrations, Li *et al.* demonstrated "quartic oscillations" in the lattice of Sc and F atoms [27]. These acoustic linkage vibrations increase in amplitude as the

[1]The quasiharmonic approximation with density functional theory for frozen phonon mode calculations and ab initio Born-Oppenheimer molecular dynamics for harmonic and anharmonic contributions respectively were used to explore this effect computationally[27].

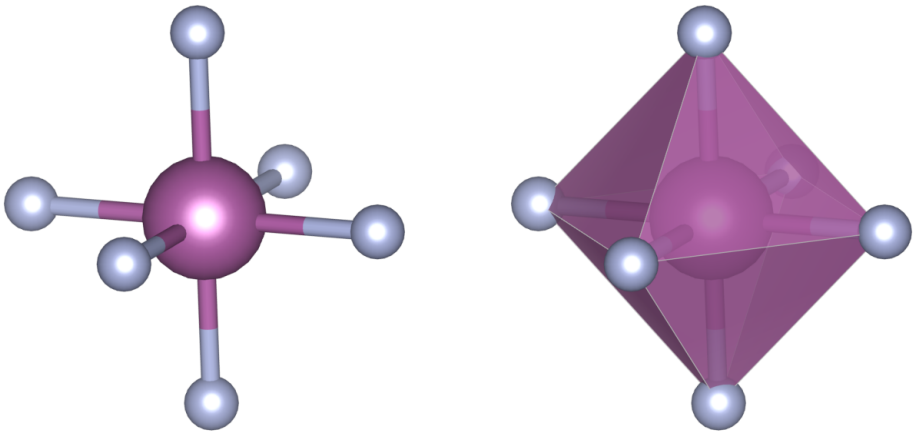

**Figure 2:** One can visualize polyhedral groups of $ScF_3$ by recasting the lattice as a collection of metal centers connected hexahedrally or octahedrally to fluoride atoms. The characteristic frequencies of these polyhedral groups are the rigid unit modes (RUMs), formed by linear combinations of the individual atomic vibrations.

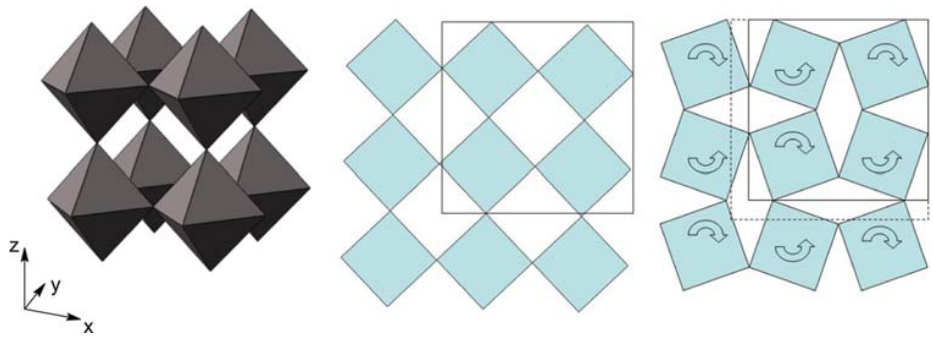


**Figure 3:** One of the possible characteristic vibrations for RUMs in a cubic system. Figure reproduced from [3]

.

temperature increases. Based on the symmetry of the structure and the way they are arranged, the larger vibrations actually pull some of the atoms closer and cause the lattice to shrink. In other words, the RUMs in $ScF_3$ are displacive and deform the shape of the lattice, resulting in a contraction of the unit cell. Not all RUM are significant; they depend on the crystal structure and symmetry. $ScF_3$ and some cubic perovskites[28] have a cubic structure responsible for not only negative thermal expansion but various phase transitions[26].

### 1.3.2 Compression Behavior

Metal fluorides are also susceptible to phase transitions under pressure. $ScF_3$ mentioned above displays a phase transition to the rhombohedral $R\bar{3}c$ phase from the cubic $Pm\bar{3}m$[29] under 0.1-0.2 GPa at 50K. Other structures undergo a phase transition from a cubic symmetry to a rhombohedral symmetry upon cooling[30]. Changes in the space group need to be considered when simulating the materials.

## *1.4 Computational Modeling of Materials*

The use of computational modeling of materials has risen with the rise of low cost computing clusters. Material modeling has become an integral part of the discovery and synthesis of new materials. Often traditional experimental approaches can lead to difficult material characterizations or synthesis difficulties due to the shear volume of possible combinations. High throughput screening has become an important technique in selecting materials to use for new applications, for example the CoreMoF database [31] or The Materials Project [32]. The computation of properties is possible via at least two methods; (1) molecular dynamics, (2) quantum methods. Quantum methods are preferred for their higher accuracy, as long as the systems to be studied are small. This work uses Kohn-Sham density functional theory (DFT), a quantum method which replaces each electron wavefunction with the electron density and solves for solutions to the Schroedinger Equation. The exchange and correlational

interactions between electrons are captured by functionals that approximate the true exchange-correlation relations. When possible, the use of prior experimental data is used for materials. This way, a potentially expensive task of finding stable materials can be done with speed and low cost.

## *1.5 Purpose and Scope of Study*

This work builds upon a prior set of experimental and computational work where negative thermal expansion was identified for cubic $CaZrF_6$ and $CaHfF_6$. These $A^{II}B^{IV}F_6$ type cubic metal fluorides were identified experimentally to have substantial negative thermal expansions of $\alpha_{L100K} \approx$ -18 and -22 ppm·$K^{-1}$ respectively [4]. DFT calculations were used to investigate the vibrational properties at 0 K using the Grüneisen parameter[4]. In this thesis, a more rigorous computational method is achieved by using the established quasi-harmonic approximation method[33] to calculate thermal expansion as a function of temperature. Since materials that display RUMs in a cubic phase tend to have negative thermal expansion, a group of materials identified as stable in the cubic $Fm\bar{3}m$ phase (225 space group) at finite temperature were selected. The thermal expansion was computed and phase stability explored for these stable cubic structures.

# CHAPTER II

# METHODS

This chapter details the computational methods used to calculate thermal expansion by studying $CaZrF_6$ as an example of a stable material experimentally known to have NTE. The three steps discussed - (1) generation of 0 K structure, (2) determination of phase stability, (3) calculation of thermal expansion as function of temperature - were repeated for all other compounds investigated, as shown in Table 2.

## *2.1 Introduction*

The $A^{II}B^{IV}F_6$ type materials that were experimentally known to be stable in the cubic $Fm\bar{3}m$ phase at room temperature[1] are shown in Table 2. These materials can be checked for stability through the use of vibrational density of states (VDOS) calculations which is explained in a later section.

## *2.2 Density Functional Theory*

The unit cell of a $A^{II}B^{IV}F_6$ metal fluoride contains 32 atoms. Finding the energy of the structure requires solving the many-body Schroedinger equation for the wave-functions of each atom and the associated energy eigenvalues. While a theoretically well formulated problem, exactly solving the equation for a system with more than three or four atoms becomes exponentially expensive and for all purposes, computationally impossible. Several approximate theories and semi-empirical methods have been developed to find an approximate solution, but the one most appropriate for the structure studied in this work is density functional theory (DFT)[34]. DFT is an ab-initio method that, unlike Hartree-Fock methods or most quantum mechanical

**Table 2:** Known Cubic $A^{II}B^{IV}F_6$ Type Materials Stable at Room Temperature [1].

| Material |
|---|
| $CaZrF_6$ |
| $CaTiF_6$ |
| $CaSnF_6$ |
| $SrSnF_6$ |
| $ZnZrF_6$ |
| $MgZrF_6$ |
| $MnZrF_6$ |
| $MgNbF_6$ |
| $MnNbF_6$ |
| $FeHfF_6$ |
| $MnHfF_6$ |
| $CaHfF_6$ |
| $CoZrF_6$ |

(QM) methods, describes the system with the electron density instead of the electronic wavefunctions. Instead of describing the system with a single Slater determinant (a gross approximation which assumes wavefunction independence), Hohenberg and Kohn proposed that the electron density uniquely determines the system and therefore the associated energy eigenvalue. In this theory, interactions between different electrons are captured by an exchange-correlation functional, and the problem becomes determining the nature of this functional.

Although it is again computationally impossible to represent the exact exchange-correlation functional, there are multiple approximations which have reasonably high accuracy for relatively low cost. The orbitals that have been treated as valence for each material is listed in Table 3. Although $MnZrF_6$, $MgNbF_6$, $MnNbF_6$, $FeHfF_6$, $FeHfF_6$, $MnHfF_6$, and $CoZrF_6$ have partially occupied orbitals, the *VASP 5.3.3*[35][36][37][38] (Vienna Ab-initio Simulation Package) was used with a projector-augmented wave (PAW) basis set for all computations.

**Table 3:** Valence Electrons

| Material | Valence Electrons |
|---|---|
| $CaZrF_6$ | $Ca(3s, 3p, 4s), Zr(4s, 4p, 5s, 4d), F(2s, 2p)$ |
| $CaTiF_6$ | $Ca(3s, 3p, 4s), Ti(4s), F(2s, 2p)$ |
| $CaSnF_6$ | $Ca(3s, 3p, 4s), Sn(2s, 2p), F(2s, 2p)$ |
| $SrSnF_6$ | $Sr(4s, 4p, 5s), Sn(2s, 2p), F(2s, 2p)$ |
| $ZnZrF_6$ | $Zn(3p, 3d), Zr(4s, 4p, 5s, 4d), F(2s, 2p)$ |
| $MgZrF_6$ | $Mg(2p, 3s), Zr(4s, 4p, 5s, 4d), F(2s, 2p)$ |
| $MnZrF_6$ | $Mn(3p, 4s, 3d), Zr(4s, 4p, 5s, 4d), F(2s, 2p)$ |
| $MgNbF_6$ | $Mg(2p, 3s), Nb(4p, 5s, 5d), F(2s, 2p)$ |
| $MnNbF_6$ | $Mn(3p, 4s, 3d), Nb(4p, 5s, 5d), F(2s, 2p)$ |
| $FeHfF_6$ | $Fe(4s, 3d), Hf(6s, 5d), F(2s, 2p)$ |
| $MnHfF_6$ | $Mn(4s, 3d), Hf(6s, 5d), F(2s, 2p)$ |
| $CaHfF_6$ | $Ca(3s, 3p, 4s), Hf(6s, 5d), F(2s, 2p)$ |
| $CoZrF_6$ | $Zr(4s, 4p, 5s, 4d), Co(4s, 3d), F(2s, 2p)$ |

### 2.2.1 Exchange-Correlation Functional

In general, two approximations for non-empirical functionals have been developed and popularly used. The first is the local-density approximation (LDA), which takes into account the local electronic density at each step of the calculation. This study used a generalized gradient approximation (GGA)[39], which considers both the local electronic density as well as the gradient of the density at each step. The specific form of GGA selected here is known as the PBE functional, named after Perdew, Burke, and Ernzerhof who proposed it in 1996 for describing solid metals. It is known to overestimate the lattice constants by 1.3% and underestimate the bulk modulus by 9% with respect to experimental findings for metals[40].

## *2.3 Bulk Structures*

The $A^{II}B^{IV}F_6$ type compounds can take on a variety of configurations at room temperature, as can be seen in Figure 4. Based on prior work with $CaZrF_6$, structures that were identified as being the most likely candidates for NTE materials were of the $Fm\bar{3}m$ space group (225), also known as $ReO_3$ type. This structure, for a $A^{II}B^{IV}F_6$

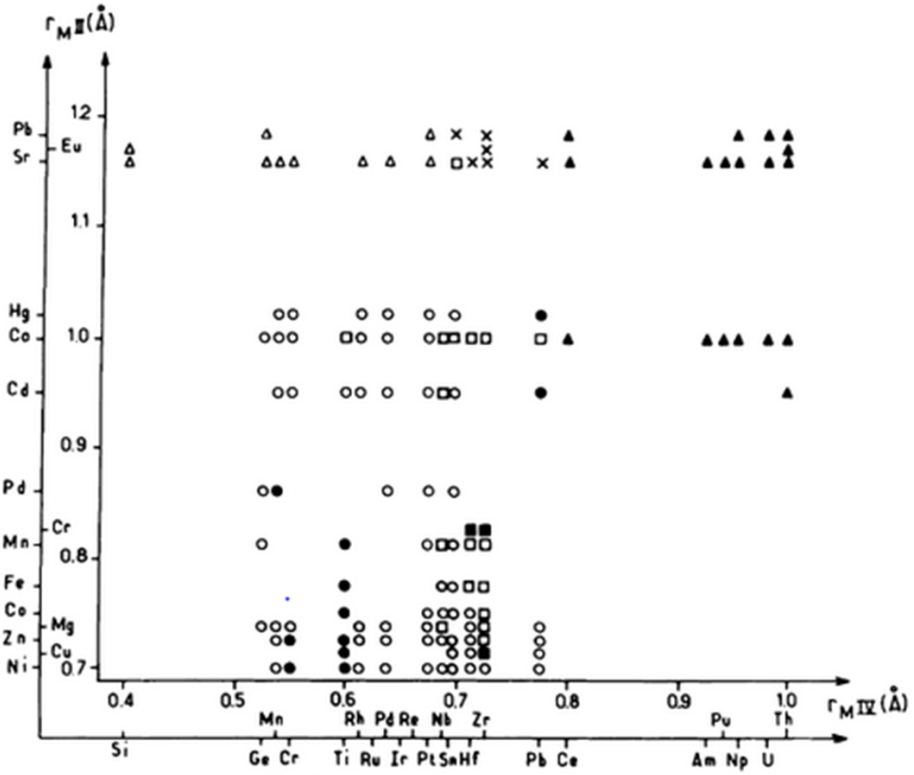


**Figure 4:** Crystallographic Structures for $A^{II}B^{IV}F_6$ at room temperature; ∘, $LiSbF_6$; • $VF_3$; □, $ReO_3$; ■, distorted $ReO_3$; ▲, $LaF_3$; △, $BaSiF_6$; and ×, various other structures. Figure reproduced from [1].

type material, has metal centers A and B coordinated with six fluorines in a cubic type pattern. As seen in Figure 5, the structure form polyhedra. The lattice vectors of this unit cell are normal to each other.

### 2.3.1 Structure Optimization

The structures were then optimized by a full relaxation of the ion positions as well as the volume and shape of the unit cell. The structure was converged to be less than 0.001 eV/Å with respect to inter atomic forces over a number of ionic steps. The electronic ground-state steps were allowed to converge to an accuracy of $10^{-8}$ eV. During each of the electronic steps, the wavefunction was improved and the charge density refined until the criterion was reached. A plane-wave energy cutoff of 600 eV was used for all calculations.

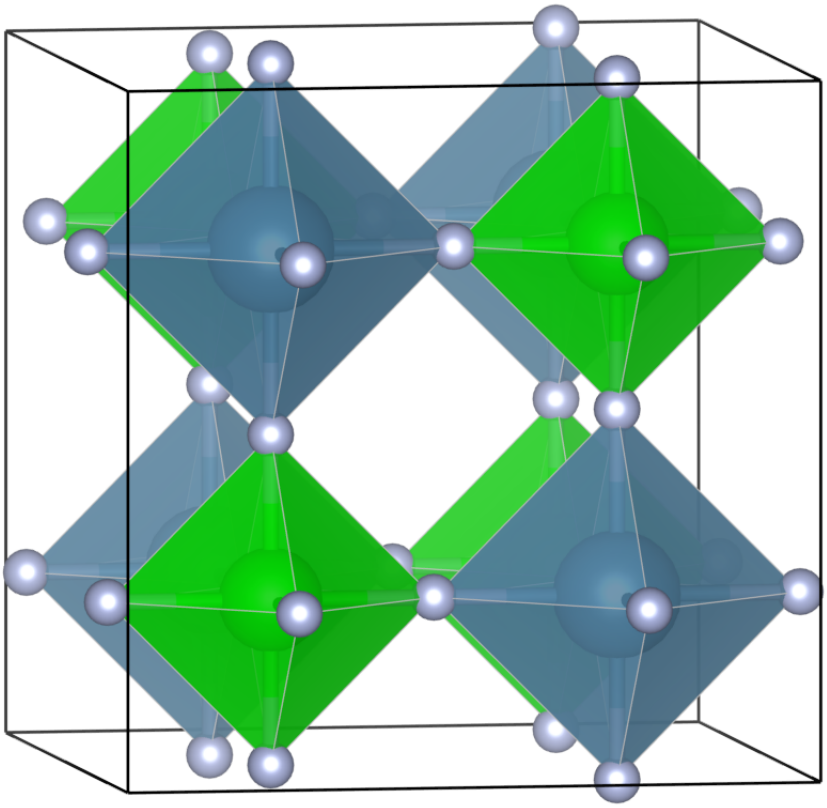

**Figure 5:** Crystallographic structure for $A^{II}B^{IV}F_6$ in space group 225.

### 2.3.2 Space Groups

The space groups for newly optimized bulk structures were identified using *pymatgen*[41]. This allowed for throughput of structures from the Inorganic Crystal Structure Database to structures that can be used by *VASP*.

## *2.4 K-Points*

Actual computation of the electron density requires numerically integrating the density of states over the primitive cell. This integration is easiest to carry out in reciprocal space where a quantized wavenumber k replaces the three-dimensional Cartesian position vector. In this reciprocal space, also known as k-space, the smallest irreducible region of space is defined as the Brillouin zone. However, numerical integration requires the definition of a mesh. The function to be integrated is evaluated at each point on the mesh. Obviously, a finer mesh will result in higher accuracy, but at the cost of computational time. A k-point sampling was performed to identify the minimum number of k-points (points on a mesh in k-space) necessary to ensure convergence. The results are shown in Figure 6, and a 8×8×8 Monkhorst-Pack (MP) grid was chosen for all simulations. To account for discontinuations in the Brillion zone, a correction developed by Methfessel-Paxton[42] was used to estimate the occupancies, with a smearing width of 0.05 eV.

## *2.5 Vibrational Density of State*

Once the converged structures for each material in the $Fm\bar{3}m$ space group were obtained, the stability of these structures at 0 K was assessed. One way to determine the stable structure for a material is to examine all of the possible space groups, and the material with the lowest energy is the stable form. This method however, requires an exhaustive search of all space groups. A calculation of this type has been done before but is typically very expensive[43]. Fortunately, since the structural

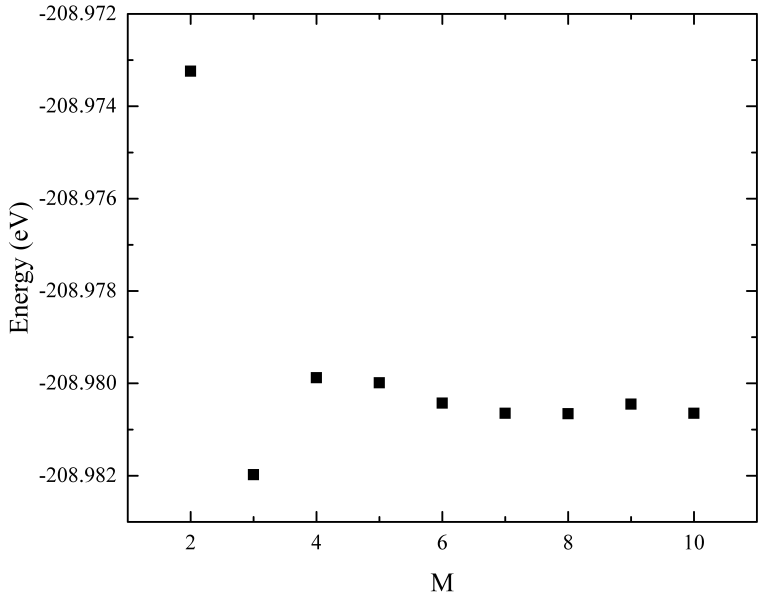


**Figure 6:** Total energy (eV) for a unit cell for bulk $CaZrF_6$ in $Fm\bar{3}m$ spacegroup where M is for calculations using M×M×M k-points.

information at room-temperature of each structure is known, we can directly evaluate the vibrational density of states (VDOS). The method utilizes a phonon calculation at 0 K to see if there are imaginary phonon modes, also called a *soft mode*. The presence of an imaginary mode indicates that the structure is unstable in the space group and there is a more stable structure[30].

### 2.5.1 VDOS Calculation

In order to access the stability of materials, the vibrational density of states (VDOS) was calculated using the software *PHONOPY* [44]. The VDOS is evaluated using a finite displacement method utilizing supercells and is based on the Parlinski-Li-Kawazoe method[45]. Displacements of 0.02 Å were used for the calculation of the force constants in the displacement method. A larger displacement was used to avoid possible numerical inaccuracies in the system.

### 2.5.2 Vibrational Density of State Theory

First, the energy of the crystal,$\phi$, with different displacements was found. $u(l\kappa)$ is the displacement of $l$ and $\kappa$ unit cell and atom. The force constants; $\phi_0$ and $\phi_{\alpha\beta}$ are the zero-th and first order [44].

$$\phi = \phi_0 + \sum_{l\kappa}\sum_{\alpha}\phi_\alpha(l\kappa)u_\alpha(l\kappa) + 1/2\sum_{ll'\kappa\kappa'}\sum_{\alpha\beta}\phi_{\alpha\beta}(l\kappa,l'\kappa')u_\alpha(l\kappa)u_\beta(l'\kappa') + ... \quad (4)$$

The phonon mode frequency was determined from a dynamical matrix made of the force constants, $m_\kappa$ atomic mass, wave vector $\mathbf{q}$, and band index $j$.

$$D(\mathbf{q})e_{\mathbf{q}j} = \omega^2_{\mathbf{q}j}\, e_{\mathbf{q}j} \quad (5)$$

Once the phonon frequencies have been found, the VDOS can be found using;

$$g(\omega) = \frac{1}{N}\sum_{\mathbf{q}j}\sigma(\omega - \omega_{\mathbf{q}j}) \quad (6)$$

The sum of these phonon modes generate the VDOS that can be seen in Figure 7. Plotted on the x-axis are the positions (in wave vectors) within the Brillouin zone of the structure. The higher energy bands are designated the "optical bands" since they interact with electromagnetic radiation. The lower energy bands are the "acoustic bands", with energies characteristic of sound waves. When one of the modes has an imaginary mode it is graphically represented as negative, for example with $CaZrF_6$, there is an acoustic mode that becomes negative in Figure 8.

The VDOS was calculated for each of the candidate materials. Those found to be unstable due to imaginary modes were not considered for the quasi-harmonic approximation as a way to reduce the computational complexity of the project. The identification of the correct space group has been shown to be non-trivial and computationally expensive.

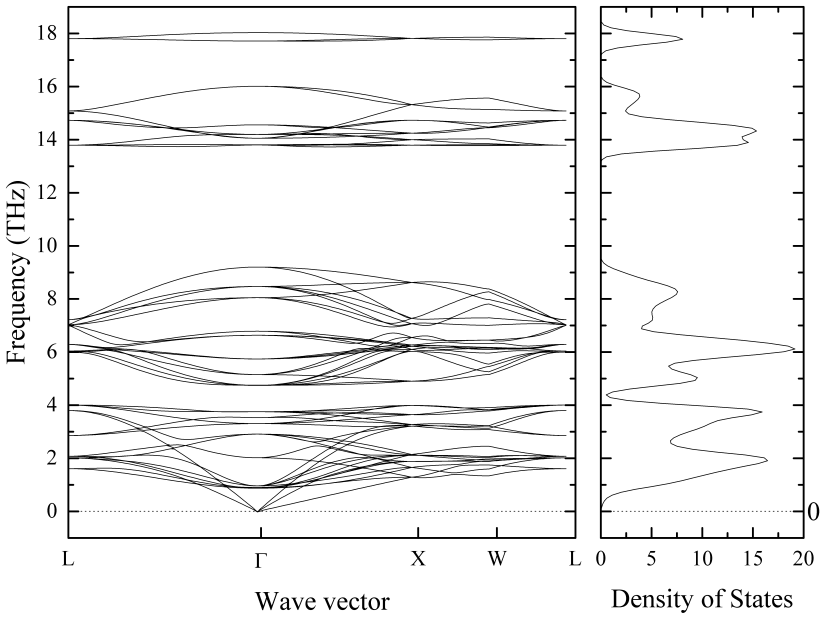


**Figure 7:** Band structure and VDOS for $CaZrF_6$ at the minimum energy point at 0 K computed within the harmonic approximation with DFT using the PBE-GGA functional.

## *2.6 Quasi-Harmonic Approximation*

The quasi-harmonic approximation is a method that allows for the computation of thermodynamic properties including the TE for a material using ab intio calculations. The method has been implemented in *phonopy-qha* part of the *PHONOPY* package.

### 2.6.1 Harmonic Approximation

The harmonic approximation comes from the assumption that movements by ions from the equilibrium position are very small. The interactions of ions therefore is similar to interconnected fixed springs. This is valid to temperatures that are well below the melting point of the structure. The crystal symmetry can be used to further reduce the number of these constants. This approximation has good agreement with the properties of solids.

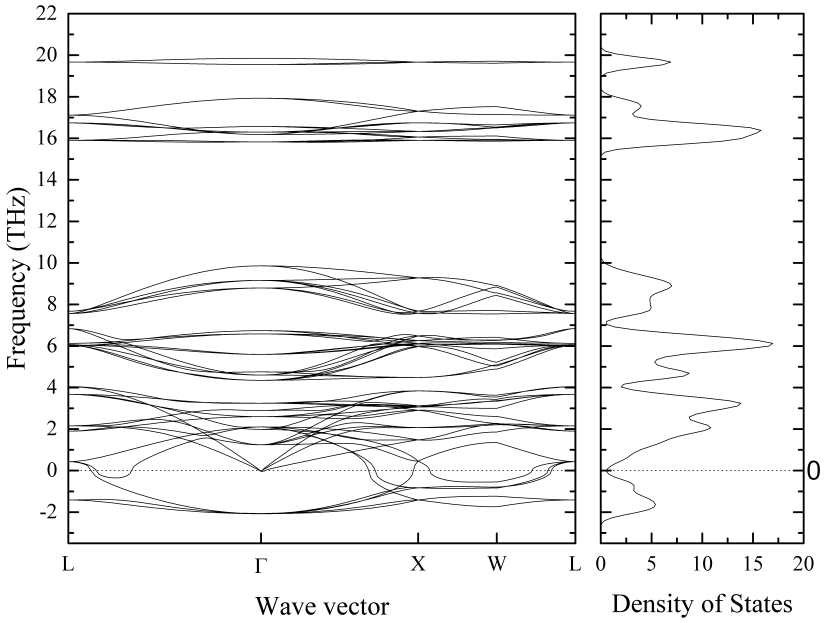


**Figure 8:** Band structure and VDOS for $CaZrF_6$ at a volume compressed by 5% at 0 K computed within the harmonic approximation with DFT using the PBE-GGA functional. Imaginary modes in the frequency are represented by negative values.

### 2.6.2 Quasi-Harmonic Approximation Calculation

Since the assumption of completely fixed ions introduces substantial errors at temperatures above 0 K that ions, we allow for the total free energy another degree of freedom through volume. Further corrections can be made, including anharmonics which account for phonon-phonon interactions but these effects are ignored here since these effects are more significant at high-temperature[46]. (1) The energies of the structure at "ground state" as a function of volume was calculated. The structures examined were over the range ± 2% for expansion and contraction. These energies were calculated with an accuracy of $10^{-8}$ eV for the electron step.

(2) The phonon contribution was added to these energies by the equation $F_{phonon}$ with temperature as a degree of freedom. These non-zero contributions occur even when the temperature is 0 K, more commonly known as zero point energy. The phonon contribution is calculated as follows:

$$F_{phonon} = \frac{1}{2}\sum_{\mathbf{q},v}\hbar\omega_{\mathbf{q},v} + k_B T\sum_{\mathbf{q},v} ln[1 - exp(-\hbar\omega_{\mathbf{q},v}/k_B T)] \quad (7)$$

where $\omega_{\mathbf{q},v}$ is the phonon frequency for a given wave vector $\mathbf{q}$ and band index $\nu$. $k_B$ is the Boltzman constant and $\hbar$ the reduced plank constant. Materials identified to be stable at 0 K from the VDOS and at room temperature experimentally in the $Fm\bar{3}m$ space group were selected. The total Gibbs free energy as a function of volume was obtained for each temperature up to 400 K at constant pressure. At steps of every 10 K, the points were fit using a least squares method to obtain the minimum energy. The minimum Gibbs free energy relates to the equilibrium volume as a function of temperature.

$$G(T,p) = \min_{V}\left[U(V) + F_{phonon}(T;V) + pV\right] \quad (8)$$

The TE and lattice parameter as a function of temperature obtained for each stable material. The dashed curve on the Gibbs free energy plot helps to guide the eye to minimums (Figure 9). These minimum points are the volumes for each temperature which are then used to find the thermal expansion coefficient using equation (1). In the example, $CaZrF_6$ is shown to have negative thermal expansion (Figures 10 and 11).

Calculations involving the quasi-harmonic approximation were done using a unit cell with displacements of 0.02 Å for the calculation of the force constants in the displacement method. A plane-wave energy cutoff of 600 eV was used with a 8×8×8 Monkhorst-Pack (MP) grid. The Methfessel-Paxton scheme[42] was used to estimate the occupancies, with a smearing width of 0.05 eV.

## *2.7 Phase Stability*

Metal fluorides of cubic structure (space group $Fm\bar{3}m$) are susceptible to pressure included phase transitions. $CaZrF_6$ has been shown to under go a phase transition when 400 MPa is applied[4]. This behavior was explored through the expansion and

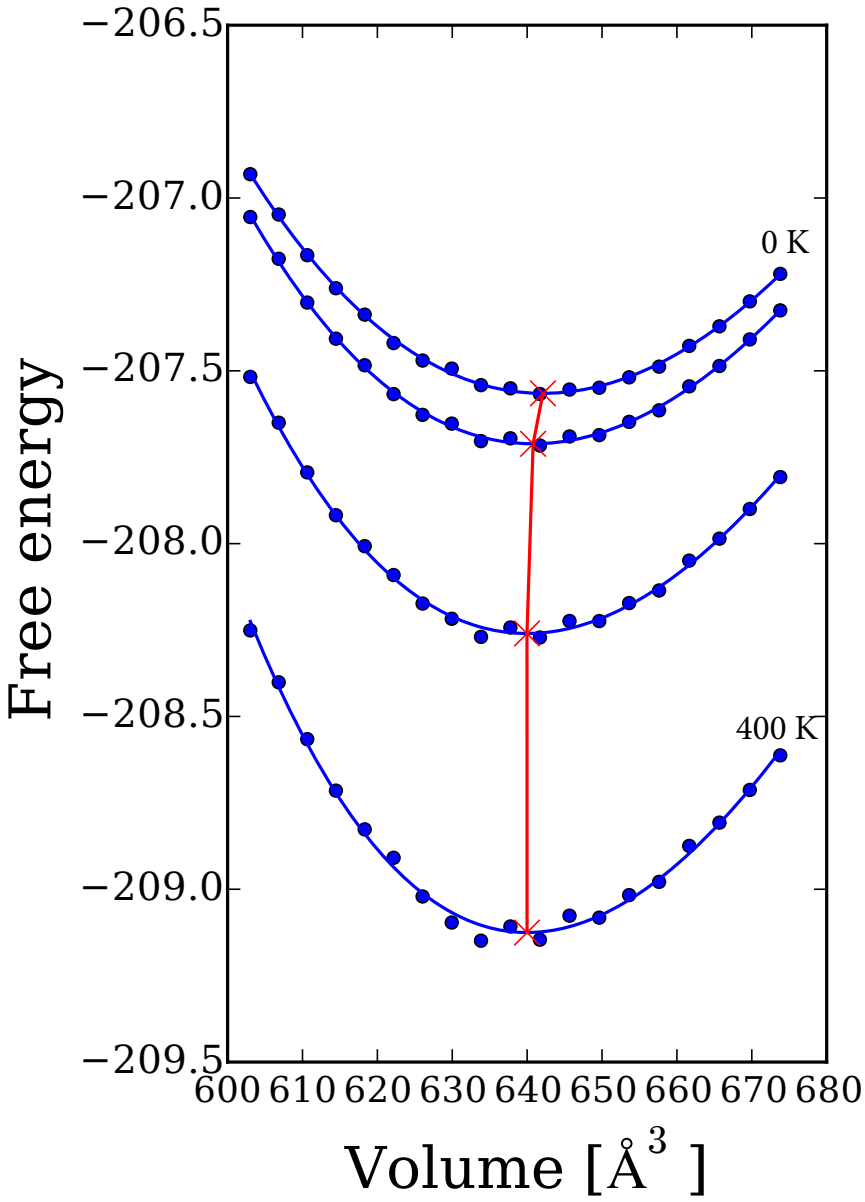


**Figure 9:** Free energy as a function of volume and temperature for $CaZrF_6$ over 0 to 400 K.

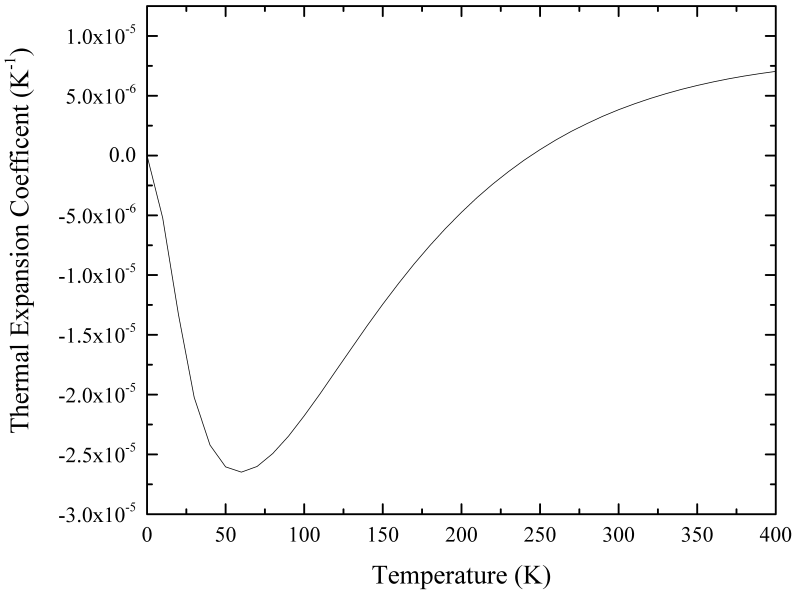


**Figure 10:** Volumetric thermal expansion coefficient for $CaZrF_6$ over 0 to 400 K.

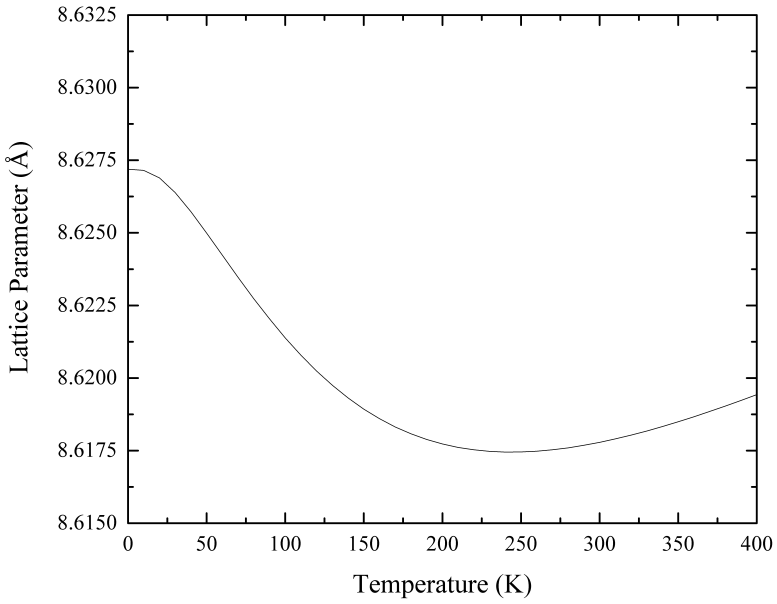


**Figure 11:** The unit cell lattice parameter for $CaZrF_6$ over 0 to 400 K.

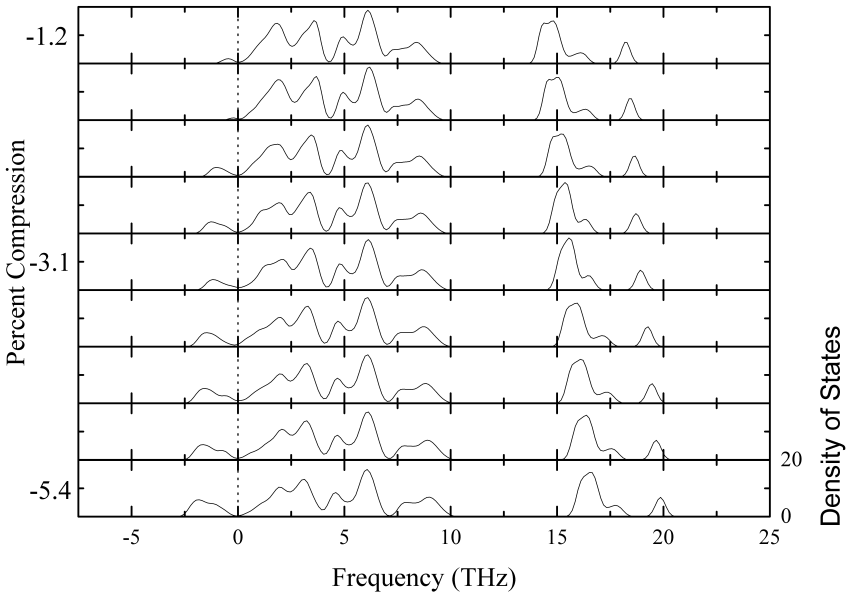


**Figure 12:** Multiple VDOS for the compression of $CaZrF_6$ structure from -1.2% to -5.4% at 0 K. Imaginary modes in the frequency are represented by negative values.

compression range generated for the quasi-harmonic approximation method. The bulk modulus was calculated using the Rose-Vinet equation of state and did not account for the zero point energy contributions, the free energy of phonons at 0 K. This is due to the error in the phonon contribution from soft modes.

The instability due to compression is closely tied to geometrical behavior of the RUMs within the structure. The effect is seen in $CaZrF_6$, where low acoustic modes near the $\Gamma$ point region develop an imaginary region (indicated by a negative mode in Figure 12). The development of this imaginary mode means that the structure is unstable and a phase transition is expected. The methods were then repeated for each of the materials listed in Table 2.

# CHAPTER III

# RESULTS AND DISCUSSION

The structures that were identified as stable at 0 K in the cubic $Fm\bar{3}m$ space group were $CaZrF_6$, $CaHf_6$, $MnZrF_6$, $MnNbF_6$, and $ZnZrF_6$. Of these structures, $CaZrF_6$ and $CaHf_6$ were previously known to exhibit NTE, as confirmed in this study. From the VDOS calculations, $ZnZrF_6$ and $MnZrF_6$ are stable in the cubic phase ($Fm\bar{3}m$) at 0 K. These materials were found to have higher energy in the $R\bar{3}$ space group, indicating the cubic phase is more stable, but there is evidence to the contrary[47]. Therefore due to this discrepancy and since $R\bar{3}$ is less likely to display modes that cause NTE, the TE of these materials are left for future inspection.

## *3.1 Stable Structure Phases*

The stabilities of $CaZrF_6$, $CaHfF_6$, and $MgNbF_6$ were investigated using the VDOS, bulk modulus, and relative energies. The bulk modulus (0 K) was found to be 75.8, 82.5, and 96.2 GPa for $CaZrF_6$, $CaHfF_6$, and $MgNbF_6$ respectively. Since the phase transition pressure of $CaZrF_6$ is known to be 400 MPa[4], the corresponding unit cell volume was explored as a function of pressure. The phase transition was estimated through the identification of unstable modes in the VDOS. Assuming that the transition pressure was constant over the range of 0-400 K, the change in unit cell volume was calculated at this pressure via the temperature dependent bulk modulus.

### 3.1.1 Space Groups

The identification of the new space groups for $CaZrF_6$ in the compressed phase was done through a comparison of the lowest energy structures. The Inorganic Crystal Structure Database was used to identify potential starting structures using known six

**Table 4:** Space groups and relative energies at 500 MPa for $CaZrF_6$

| Space Group | International Notation | Energy (eV/atom) | Initial Structures |
|---|---|---|---|
| 2 | $P\bar{1}$ | -6.012 | $CuSnF_6$ [48] |
| 51 | $Pmma$ | -6.045 | $SrThBr_6$ [49] |
| 62 | $Pnma$ | -6.010 | $NaCrF_6$ [50] |
| 67 | $Cmme$ | -6.072 | $PbZrF_6$ [51] |
| 84 $\rightarrow$ 132 | $P4_2/m \rightarrow P4_2/mcm$ | -6.040 | $NaSbCl_6$ [52] |
| 111 $\rightarrow$ 132 | $P\bar{4}2m \rightarrow P4_2/mcm$ | -6.040 | $KSbF_6$ [53] |
| 116 $\rightarrow$ 132 | $P\bar{4}c2 \rightarrow P4_2/mcm$ | -6.040 | $KNbF_6$ [54] |
| 131 | $P4_2/mmc$ | -5.727 | $SrPbF_6$ [55] |
| 132 | $P4_2/mcm$ | -6.039 | $KSbF_6$ [53] |
| 139 $\rightarrow$ 225 | $14/mmm \rightarrow Fm\bar{3}m$ | -5.929 | $CrNbF_6$ [56] |
| 146 $\rightarrow$ 148 | $R3 \rightarrow R\bar{3}$ | -5.943 | $LiWCl_6$ [57] |
| 148 | $R\bar{3}$ | -5.943 | $KAsF_6$ [58] |
| 166 | $R\bar{3}m$ | -5.919 | $BaTiF_6$ [59] |
| 205 | $Pa\bar{3}$ | -5.929 | $NaSbF_6$ [60] |
| 206 | $Ia\bar{3}$ | -6.015 | $AgSbF_6$ [61] |
| 225 | $Fm\bar{3}m$ | -5.929 | - |

coordinated metal complexes (Table 4). The structures were optimized at a pressure of 500 MPa. Of these space groups; 84, 11, 116, 139, and 146 were found to transition to another group during optimization. A space group transition indicates that the original space group is not the most stable at the calculation pressure, and therefore the material will shift to a lowest energy state. The stoichiometry of each structure is an integer multiple of the $CaZrF_6$ stoichiometry so the energies are reported in eV per atom for direct comparison. Space group 67 ($Cmme$) was found to have the lowest energy and consequently, the most stable structure of those examined.

### 3.1.2 Phase Transition

By identifying the formation of unstable modes under system compression, the phase transition pressure of $CaZrF_6$ was calculated to be 475 MPa. Once these modes appeared, the bulk modulus was used to find the corresponding system pressure. The result of this process can be seen in Figure 13 where the unit cell volume at the phase

transition is compared with the energy minimum volume. The lines in Figure 13 are isobaric with respect to temperature. The 0 MPa line of cell volume as function of temperature is the result from the quasi-harmonic approximation. The transition line (475 MPa) was calculated using the temperature dependent bulk modulus with the assumption of a constant transition pressure. The space group that was identified for $CaZrF_6$ was *Cmme* (67), this is an orthorhombic space group which means that for the unit cell, sides $a \neq b \neq c$ with angles of 90°. Therefore, without determining the structure at 466 MPa we cannot precisely determine the lattice parameters at the transition pressure. The transition behavior is explored as a function of volume and temperature in Figure 13. At 500 MPa and 0 K the lattice parameters for the *Cmme* space group describe an orthorhombic structure with $a = 5.1368$, $b = 7.4809$, and $c = 10.4848$ Å. The structure is shown in Figure 14. Interestingly, coordination of fluorines to a central zirconium increases from six to eight, due to the large ionic radius of the high valence shell of the metal. This behavior is similar to that seen in other zirconium(IV) flouride complexes [62][63][64].

The transition pressure for $CaHfF_6$ was identified as 466 MPa respectively. The pressure was identified from the free energy-volume calculation in the quasi-harmonic approximation. After the structure was compressed, soft modes developed, indicative of a pressure induced phase transition. Figure 15 demonstrates the variation of the unit cell volume for $CaHfF_6$. Once again, the line a 0 MPa indicates the minimum energy volume as a function of temperature. For $CaHfF_6$, the unit cell volume required a compression of about 3.5 $Å^3$ to enable a pressure induced phase transition in the cubic structure. This difference, between the minimum energy and phase transition volumes, decreased to roughly 2 $Å^3$ at 400 K. This corresponds to a hardening of the materials following a compression due to the increase in temperature.

$MgNbF_6$ demonstrated stability at 0 K for the cubic space group with a pressure induced phase transition at around 526.9 MPa. The change in unit cell volume was

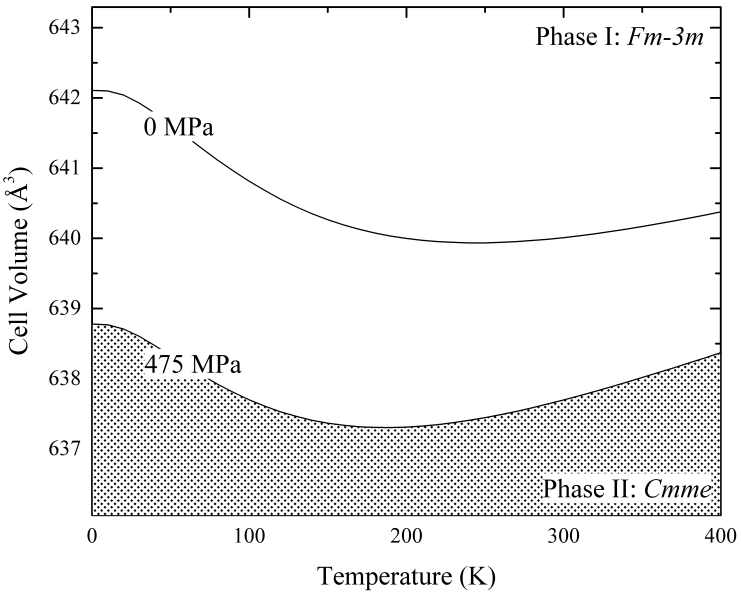


**Figure 13:** The phase transition behavior for $CaZrF_6$ over 0 to 400 K.

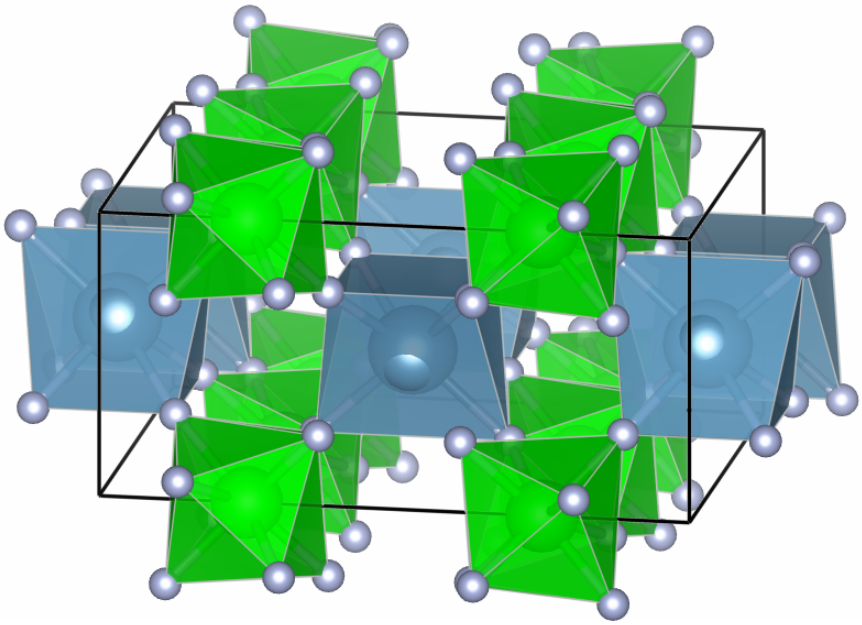

**Figure 14:** The pressure induced *Cmme* space group was found at a pressure of 500 MPa at 0 K. The initial structure was of the form of $PbZrF_6$ from the Inorganic Crystal Structure Database.

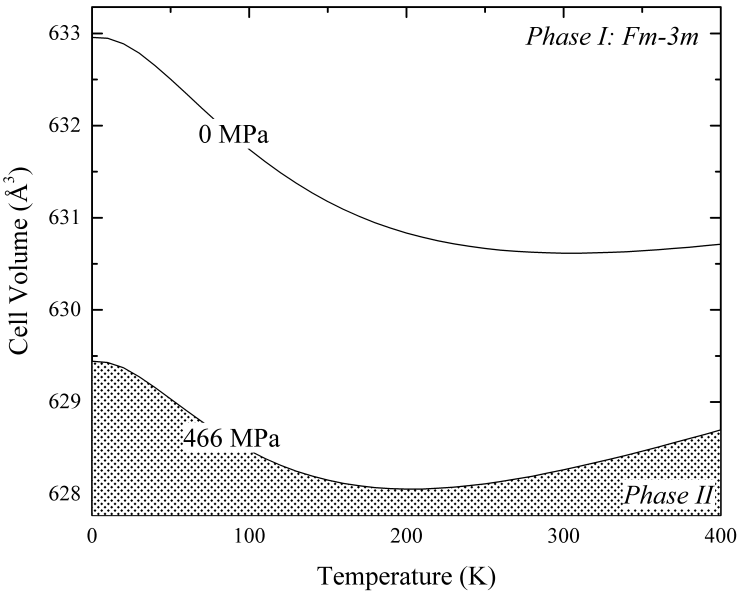


**Figure 15:** The phase transition behavior for $CaHfF_6$ over 0 to 400 K.

found to be much smaller over the temperature range than the two previous hexafluoride complexes (see Figure 16). The slight negative thermal expansion coefficient with the low acoustic bands is indicative of RUM that has been used to describe the NTE behavior of $CaHfF_6$. This composition was also considerably harder than $CaZrF_6$ and $CaHfF_6$ and therefore more resistant to a phase transition from pressure.

$ZnZrF_6$ and $MnZrF_6$ were identified to be stable in the cubic phase ($Fm\bar{3}m$) at 0 K. These materials are expected to have lower energy in the $R\bar{3}$ space group but there is evidence otherwise. $ZnZrF_6$ was shown to undergo a phase transition at 310 K to the rhombohedral structure [47]. However, calculations comparing $ZnZrF_6$ with $MnZrF_6$ directly contradict this experimental conclusion. A VDOS calculation at 0 K finds that $ZnZrF_6$ has energies of -5.57 and -5.01 $\frac{eV}{atom}$ for $Fm\bar{3}m$ and $R\bar{3}$ respectively, indicating that the $Fm\bar{3}m$ phase is more stable. Similarly, a VDOS calculation on $MnZrF_6$ resulted in energies of -6.45 and -5.96 $\frac{eV}{atom}$ for space groups $Fm\bar{3}m$ and $R\bar{3}$,

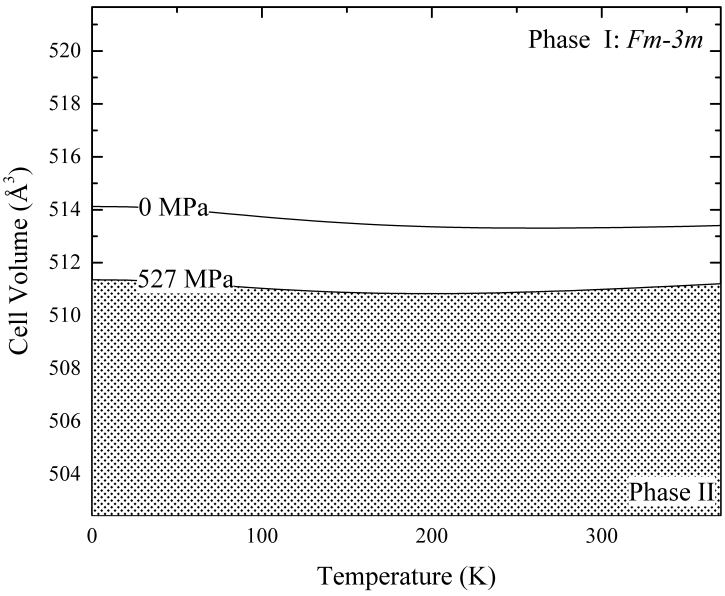


**Figure 16:** The phase transition behavior for $MgNbF_6$ over 0 to 400 K.

where the $Fm\bar{3}m$ phase again was lower energy and therefore more stable. This discrepancy between the stability measured experimentally and the calculations requires further investigation. The stability may be the result a low temperature effect that is occurring in these materials. For $MnZrF_6$ in particular, additional attention should be given to the magnetic moment due to spin polarization.

## *3.2 Thermal Expansion*

The volumetric thermal expansions for $CaZrF_6$,$CaHfF_6$, and $MgNbF_6$ were found to be $\alpha_{100K}$ = -2.177×$10^{-5}$, -2.17×$10^{-5}$, and -1.091×$10^{-5}$ $K^{-1}$respectively. Each display NTE over 0-200 K where $CaZr_6$ was found to have the greatest TE followed by $CaHfF_6$ and $MgNbF_6$ (Figure 17). The computed thermal expansion data is compared to experimental results in Figures 18 and 19. In both cases, the negative thermal expansion was found to be much smaller in comparison to experimental data. For $CaZrF_6$, the experimental linear TE was $\alpha_{100K} \sim$ -1.8×$10^{-5}$ $K^{-1}$ (From

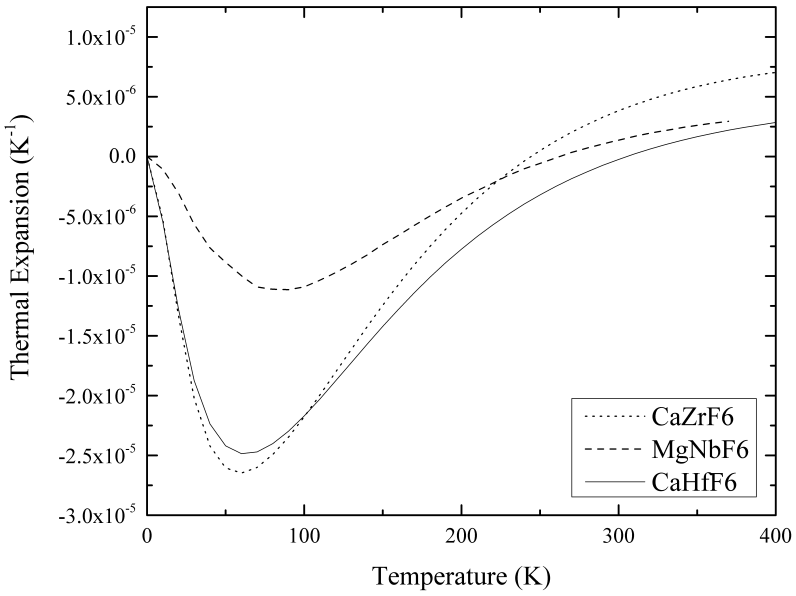


**Figure 17:** The volumetric thermal expansion coefficient for $CaZrF_6$, $CaHfF_6$, and $MgNbF_6$ over 0 to 400 K in (225) cubic phase.

this paper, a linear CTE of $\alpha_{100K} \sim$ -7.26 $\times 10^{-6}$ $K^{-1}$). $CaHfF_6$ was also predicted to have stronger NTE than experimentally found at $\alpha_{100K} \sim$ -2.2$\times 10^{-5}$ $K^{-1}$ (From this paper, a linear CTE of $\alpha_{100K} \sim$ -7.23 $\times 10^{-6}$ $K^{-1}$).

The discrepancies between the TE generated from the quasi-harmonic approximation and the experimental values are largely due to the instabilities in the structure. As demonstrated, each material undergoes a pressure induced phase transition. When the structure is compressed, for the quasi-harmonic approximation, soft acoustic modes are generated at the lowest bands around the $\Gamma$ point. These unstable modes produce imaginary contributions to the that are later ignored in the phonon energy contributions (Equation 7). The contribution of errors increases with temperature due to the summation in the second term over the modes. Large fluctuations in the Gibbs free energy can be generated above 0 K that cause alterations of the lowest energy state volume. The combination of these errors causes the significant

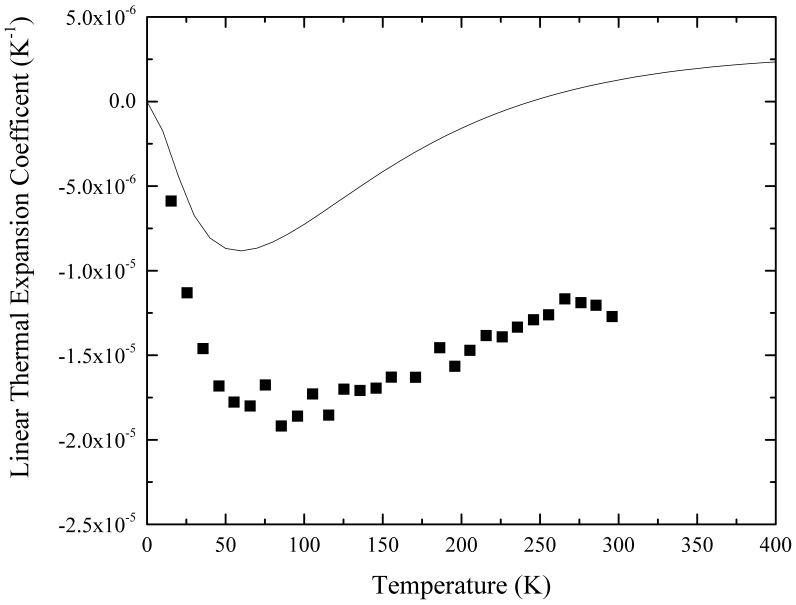


**Figure 18:** Comparison of the linear thermal expansion to experimental results[4] for $CaZrF_6$, indicated by ■.

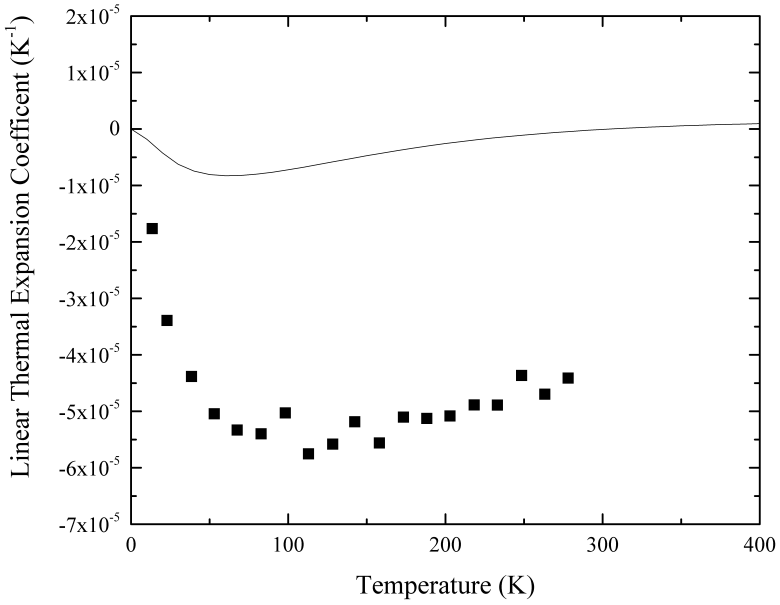


**Figure 19:** Comparison of the linear thermal expansion to experimental results[4] for $CaHfF_6$, indicated by ■.

difference in TE between the simulated and experimental results.

Despite the error contributions, the methods within this thesis replicated the results from experiment to demonstrate NTE. Additionally, $MgNbF_6$ was identified as a strong candidate for NTE with near ZTE properties. In future calculations, the anharmonic contributions must be accounted as the quasi-harmonic approximation generates large errors.

# CHAPTER IV

# CONCLUSION

The stability and thermal expansion of thirteen materials was evaluated using density functional theory methods that included vibrational density of state calculations, quasi-harmonic approximation, derived thermodynamic quantities, and phase stability analysis. Of these, $CaZrF_6$, $CaHfF_6$, and $MgNbF_6$ were demonstrated to have both the desirable property of negative thermal expansion and stability at 0 K. The thermal expansions for $CaZrF_6$,$CaHfF_6$, and $MgNbF_6$ were found to be $\alpha_{100K}$ = -2.177$\times10^{-5}$, -2.17$\times10^{-5}$, and -1.091$\times10^{-5}$ $K^{-1}$ respectively. The $CaZrF_6$ and $CaHfF_6$ coefficients were compared to experimental thermal expansion coefficients and found to be under predicting. This underestimation was determined to be due to, in part, the formation of the unstable phonon modes and their lack of contribution to the energies. In future work, the anharmonic contributions must be accounted for to identify NTE materials with pressure instabilities at accuracy. The stability of these structures was also explored. Pressure induced phase transitions were predicted to occur at pressures beyond 475 MPa, 466 MPa, and 526.9 MPa for $CaZrF_6$, $CaHfF_6$, and $MgNbF_6$ respectively. These transitions occurred due to the introduction of the soft modes in the low acoustic modes of band structure.

Future work could involve an exhaustive search of all metal combinations of $A^{II}B^{IV}F_6$. This has the potential to identify new stable metal hexaflourides. The identification of new metal fluoride formulations would provide additional materials to aid in the design of modern electronics and fiber optics. Controlling the thermal expansion of materials has great potential. Since the thermal expansion can be controlled through chemical substitutions, particle size, pressure and strain, and defects,

application specific material design methods is possible once these contributing effects are easily determined.

# REFERENCES


[1] P. Hagenmuller, *Inorganic Solid Fluorides: Chemistry and Physics*. Elsevier, 2012.

[2] J. Chen, F. Wang, Q. Huang, L. Hu, X. Song, J. Deng, R. Yu, and X. Xing, "Effectively control negative thermal expansion of single-phase ferroelectrics of $PbTiO_3$-(Bi,La)$FeO_3$ over a giant range," *Sci Rep*, vol. 3, 2013.

[3] W. Miller, C. Smith, D. Mackenzie, and K. Evans, "Negative thermal expansion: a review," *J Mater Sci*, vol. 44, no. 20, pp. 5441–5451, 2009.

[4] J. C. Hancock, K. W. Chapman, G. J. Halder, C. R. Morelock, B. S. Kaplan, L. C. Gallington, A. Bongiorno, C. Han, S. Zhou, and A. P. Wilkinson, "Large negative thermal expansion and anomalous behavior on compression in cubic $ReO_3$-type $A^{II}B^{IV}F_6$: $CaZrF_6$ and $CaHfF_6$," *Chem Mater*, 2015.

[5] N. Lock, Y. Wu, M. Christensen, L. J. Cameron, V. K. Peterson, A. J. Bridgeman, C. J. Kepert, and B. B. Iversen, "Elucidating negative thermal expansion in MOF-5," *J Phys Chem C*, vol. 114, no. 39, pp. 16181–16186, 2010.

[6] D. Dubbeldam, K. S. Walton, D. E. Ellis, and R. Q. Snurr, "Exceptional negative thermal expansion in isoreticular metal-organic frameworks," *Angew Chem Int Ed Engl*, vol. 119, no. 24, pp. 4580–4583, 2007.

[7] P. Lightfoot, D. A. Woodcock, M. J. Maple, L. A. Villaescusa, and P. A. Wright, "The widespread occurrence of negative thermal expansion in zeolites," *J Mater Chem.*, vol. 11, pp. 212–216, 2001.

[8] T. A. Mary, J. S. Evans, T. Vogt, and A. W. Sleight, "Negative thermal expansion from 0.3 to 1050 kelvin in $ZrW_2O_8$," *Science*, vol. 272, no. 5258, pp. 90–92, 1996.

[9] V. Korthuis, N. Khosrovani, A. W. Sleight, N. Roberts, R. Dupree, and W. W. J. Warren, "Negative thermal expansion and phase transitions in the $ZrV_{2-x}P_xO_7$ series," *Chem Mater*, vol. 7, no. 2, pp. 412–417, 1995.

[10] Y. Zhou, S. Adams, R. P. Rao, D. D. Edwards, A. Neiman, and N. Pestereva, "Charge Transport by Polyatomic Anion Diffusion in $Sc_2(WO_4)_3$," *Chem Mater*, vol. 20, no. 20, pp. 6335–6345, 2008.

[11] A. L. Goodwin, M. Calleja, M. J. Conterio, M. T. Dove, J. S. Evans, D. A. Keen, L. Peters, and M. G. Tucker, "Colossal positive and negative thermal expansion in the framework material $Ag_3[Co(CN)_6]$," *Science*, vol. 319, no. 5864, pp. 794–797, 2008.

[12] Y. Liu, Z. Wang, M. Wu, Q. Sun, M. Chao, and Y. Jia, "Negative thermal expansion in isostructural cubic $ReO_3$ and $ScF_3$: A comparative study," *Comput Mater Sci*, vol. 107, pp. 157 – 162, 2015.

[13] J. R. Salvador, F. Guo, T. Hogan, and M. G. Kanatzidis, "Zero thermal expansion in YbGaGe due to an electronic valence transition," *Nature*, vol. 425, no. 6959, pp. 702–705, 2003.

[14] F. Cverna, *ASM ready reference: thermal properties of metals*. ASM International, 2002.

[15] M. M. Salama and S. L. Wilson, "Liquefied natural gas pipeline with near zero coefficient of thermal expansion," Feb 2013. US Patent 8,365,776.

[16] J. S. Evans, "Negative thermal expansion materials," *J Chem Soc, Dalton Trans*, no. 19, pp. 3317–3326, 1999.

[17] M. J. Dejneka, C. L. Chapman, and S. T. Misture, "Strong, low thermal expansion niobate ceramics," *J Am Ceram Soc*, vol. 94, no. 8, pp. 2249–2261, 2011.

[18] A. Atkinson, S. Barnett, R. J. Gorte, J. Irvine, A. J. McEvoy, M. Mogensen, S. C. Singhal, and J. Vohs, "Advanced anodes for high-temperature fuel cells," *Nat Mater*, vol. 3, no. 1, pp. 17–27, 2004.

[19] S. Tawfick, M. De Volder, D. Copic, S. J. Park, C. R. Oliver, E. S. Polsen, M. J. Roberts, and A. J. Hart, "Engineering of micro- and nanostructured surfaces with anisotropic geometries and properties," *Adv Mater*, vol. 24, no. 13, pp. 1628–1674, 2012.

[20] V. Ravi, S. Firdosy, T. Caillat, E. Brandon, K. Van Der Walde, L. Maricic, and A. Sayir, "Thermal expansion studies of selected high-temperature thermoelectric materials," *J Electron Mater*, vol. 38, no. 7, pp. 1433–1442, 2009.

[21] J. Blendell and R. Coble, "Measurement of stress due to thermal expansion anisotropy in $Al_2O_3$," *J Am Ceram Soc*, vol. 65, no. 3, pp. 174–178, 1982.

[22] J. S. Evans, Z. Hu, J. Jorgensen, D. Argyriou, S. Short, and A. Sleight, "Compressibility, phase transitions, and oxygen migration in zirconium tungstate, $ZrW_2O_8$," *Science*, vol. 275, no. 5296, pp. 61–65, 1997.

[23] K. Wang and R. R. Reeber, "The role of defects on thermophysical properties: thermal expansion of V, Nb, Ta, Mo and W," *Mater Sci Eng R Rep*, vol. 23, no. 3, pp. 101–137, 1998.

[24] J. Chen, L. Hu, J. Deng, and X. Xing, "Negative thermal expansion in functional materials: controllable thermal expansion by chemical modifications," *Chem Soc Rev*, vol. 44, no. 11, pp. 3522–3567, 2015.

[25] L. Van Uitert, H. O'Bryan, H. Guggenheim, R. Barns, and G. Zydzik, "Correlation of the thermal expansion coefficients of rare earth and transition metal oxides and fluorides," *Mater Res Bull*, vol. 12, no. 4, pp. 307–314, 1977.

[26] M. T. Dove, "Theory of displacive phase transitions in minerals," *Am Mineral*, vol. 82, no. 3, pp. 213–244, 1997.

[27] C. W. Li, X. Tang, J. A. Muñoz, J. B. Keith, S. J. Tracy, D. L. Abernathy, and B. Fultz, "Structural relationship between negative thermal expansion and quartic anharmonicity of cubic $ScF_3$," *Phys Rev Lett*, vol. 107, p. 195504, Nov 2011.

[28] A. K. A. Pryde, K. D. Hammonds, M. T. Dove, V. Heine, J. D. Gale, and M. C. Warren, "Origin of the negative thermal expansion in $zrw_2o_8$ and $zrv_2o_7$," *J Phys: Conden Matter*, vol. 8, no. 50, p. 10973, 1996.

[29] B. K. Greve, K. L. Martin, P. L. Lee, P. J. Chupas, K. W. Chapman, and A. P. Wilkinson, "Pronounced negative thermal expansion from a simple structure: cubic $ScF_3$," *J Am Chem Soc*, vol. 132, no. 44, pp. 15496–15498, 2010.

[30] R. Cowley, "Structural phase transitions I. Landau theory," *Adv Phys*, vol. 29, no. 1, pp. 1–110, 1980.

[31] Y. G. Chung, J. Camp, M. Haranczyk, B. J. Sikora, W. Bury, V. Krungleviciute, T. Yildirim, O. K. Farha, D. S. Sholl, and R. Q. Snurr, "Computation-ready, experimental metal–organic frameworks: A tool to enable high-throughput screening of nanoporous crystals," *Chem Mater*, vol. 26, no. 21, pp. 6185–6192, 2014.

[32] A. Jain, S. P. Ong, G. Hautier, W. Chen, W. D. Richards, S. Dacek, S. Cholia, D. Gunter, D. Skinner, G. Ceder, and K. A. Persson, "The Materials Project: A materials genome approach to accelerating materials innovation," *APL Mat*, vol. 1, no. 1, p. 011002, 2013.

[33] R. Levy, A. Srinivasan, W. Olson, and J. McCammon, "Quasi-harmonic method for studying very low frequency modes in proteins," *Biopolymers*, vol. 23, no. 6, pp. 1099–1112, 1984.

[34] R. Catlow, A. Sokol, and A. Walsh, *Computational approaches to energy materials*. John Wiley & Sons, 2013.

[35] G. Kresse and J. Hafner, "*Ab initio* molecular dynamics for liquid metals," *Phys Rev B*, vol. 47, pp. 558–561, Jan 1993.

[36] G. Kresse and J. Hafner, "*Ab initio* molecular-dynamics simulation of the liquid-metal—amorphous-semiconductor transition in germanium," *Phys Rev B*, vol. 49, pp. 14251–14269, May 1994.

[37] G. Kresse and J. Furthmüller, "Efficiency of ab-initio total energy calculations for metals and semiconductors using a plane-wave basis set," *Comput Mater Sci*, vol. 6, no. 1, pp. 15–50, 1996.

[38] G. Kresse and J. Furthmüller, "Efficient iterative schemes for *ab initio* total-energy calculations using a plane-wave basis set," *Phys Rev B*, vol. 54, pp. 11169–11186, Oct 1996.

[39] J. P. Perdew, K. Burke, and M. Ernzerhof, "Generalized gradient approximation made simple," *Phys Rev Lett*, vol. 77, no. 18, p. 3865, 1996.

[40] G. I. Csonka, J. P. Perdew, A. Ruzsinszky, P. H. Philipsen, S. Lebègue, J. Paier, O. A. Vydrov, and J. G. Ángyán, "Assessing the performance of recent density functionals for bulk solids," *Phys Rev B*, vol. 79, no. 15, p. 155107, 2009.

[41] S. P. Ong, W. D. Richards, A. Jain, G. Hautier, M. Kocher, S. Cholia, D. Gunter, V. L. Chevrier, K. A. Persson, and G. Ceder, "Python Materials Genomics (pymatgen): A robust, open-source python library for materials analysis," *Comput. Mater. Sci.*, vol. 68, pp. 314 – 319, 2013.

[42] M. Methfessel and A. T. Paxton, "High-precision sampling for brillouin-zone integration in metals," *Phys Rev B*, vol. 40, pp. 3616–3621, Aug 1989.

[43] C. J. Pickard and R. Needs, "*Ab initio* random structure searching," *J Phys Condens Matter*, vol. 23, no. 5, p. 053201, 2011.

[44] A. Togo and I. Tanaka, "First principles phonon calculations in materials science," *Scr Mater*, vol. 108, pp. 1 – 5, 2015.

[45] K. Parlinski, Z. Q. Li, and Y. Kawazoe, "First-principles determination of the soft mode in cubic $ZrO_2$," *Phys Rev Lett*, vol. 78, no. 21, p. 4063, 1997.

[46] N. W. Ashcroft and N. D. Mermin, "Solid state physics," p. 293, 1976.

[47] V. Rodriguez, M. Couzi, A. Tressaud, J. Grannec, J. Chaminade, and C. Ecolivet, "Structural phase transition in the ordered fluorides $M^{II}ZrF_6$ ($M^{II}$=Co,Zn). II. Brillouin and Raman scattering study," *J Phys Condens Matter*, vol. 2, no. 36, p. 7387, 1990.

[48] B. G. Müller and F. Schrötter, "Zur kristallstruktur ternärer Cu(II)-Fluoride $CuM^{IV}F_6$ ($M^{IV}$ = Sn, Pb, Ti, Mn, Pd)," *Z Kristallogr*, vol. 196, pp. 261–268, 1991.

[49] H. P. Beck and F. Kühn, "Studies on $ABX_6$ compounds. II. The $BaThBr_6$ structure type," *Z Anorg Allg Chem*, vol. 621, no. 10, pp. 1649–1654, 1995.

[50] Z. Mazej and E. Goreshnik, "Alkali metal (Li+Cs+) salts with hexafluorochromate(V), hexafluorochromate(IV), pentafluorochromate(IV), and undecafluorodichromate(IV) anions," *Eur J Inorg Chem*, vol. 2008, no. 11, pp. 1795–1812, 2008.

[51] J. Laval, D. Mercurio Lavaud, and B. Gaudreau, "Synthesis and structural of fluorozirconates M(II)$ZrF_6$ (M(II) Pb, Sr, Eu, Ba)," *Rev Chim Miner*, vol. 11, no. 6, pp. 742–750, 1974.

[52] H. Henke, "Zur kristallchemischen einordnung von $NaSbCl_6$, $NaNbCl_6$ und $NaTaCl_6$," *Z Kristallogr*, vol. 198, pp. 1–16, 1992.

[53] G. J. Kruger, C. W. F. T. Pistorius, and A. M. Heyns, "Potassium hexafluoroantimonate (I)," *Acta Crystallogr B*, vol. 32, pp. 2916–2918, Oct 1976.

[54] H. Bode and V. D

[55] R. Hoppe and K. Blinne, "Erdalkalihexafluoroplumbate(IV)," *Z Anorg Allg Chem*, vol. 293, no. 5-6, pp. 251–263, 1958.

[56] F. Goubard, J. Chassaing, D. Bizot, and M. Quarton, "Synthesis, structural and spectroscopic studies of Cr(II)Nb(IV)$F_6$," *Eur J Solid State Inorg Chem*, vol. 31, no. 3, pp. 223–233, 1994.

[57] M. Weisser, S. Tragl, and H.-J. Meyer, "Crystal structure of lithium hexachlorotungstate(V), $LiWCl_6$," *Z Krist - New Cryst St*, vol. 223, pp. 5–6, 2008.

[58] G. Gafner and G. J. Kruger, "Potassium arsenic hexafluorine: a redetermination," *Acta Crystallogr B*, vol. 30, pp. 250–251, Jan 1974.

[59] S. Becker, G. Benner, and R. Hoppe, "Zur kenntnis des K[$OsF_6$]-Typs: Über die konstitution von $BaSnF_6$ und $BaTiF_6$," *Z Anorg Allg Chem*, vol. 591, no. 1, pp. 7–16, 1990.

[60] N. Schrewelius, "Röntgenuntersuchung der Verbindungen $NaSb(OH)_6$, $NaSbF_6$, $NaSbO_3$ und gleichartiger Stoffe," *Z Anorg Allg Chem*, vol. 238, no. 2-3, pp. 241–254, 1938.

[61] K. Matsumoto, R. Hagiwara, Y. Ito, and O. Tamada, "Crystal structures of $AgAF_6$ (A = P, As, Sb, Nb, Ta) at ambient temperatures," *J Fluor Chem*, vol. 110, no. 2, pp. 117 – 122, 2001. Solid State Inorganic Fluorides.

[62] F. Calderazzo, U. Englertb, C. Maichle-Mssmer, F. Marchetti, G. Pampaloni, D. Petroni, C. Pinzino, J. Strhle, and G. Tripepi, "Eight—coordinate chelate complexes of zirconium(IV) and niobium(IV): X-ray diffractometric and EPR investigations," *Inorg Chim Acta*, vol. 270, no. 12, pp. 177 – 188, 1998.

[63] L. M. Toth, A. S. Quist, and G. E. Boyd, "Raman spectra of zirconium(IV) fluoride complex ions in fluoride melts and polycrystalline solids," *J Phys Chem*, vol. 77, no. 11, pp. 1384–1388, 1973.

[64] K. Adil, M. Leblanc, V. Maisonneuve, and P. Lightfoot, "Structural chemistry of organically—templated metal fluorides," *Dalton Trans.*, vol. 39, pp. 5983–5993, 2010.

[65] J.-P. Laval, R. Papiernik, and B. Frit, "$BaZrF_{6\alpha}$: une structure à anion complexe $[Zr_2F_{12}]^{4-}$," *Acta Crystallogr B*, vol. 34, pp. 1070–1074, Apr 1978.

[66] J.-S. Zhou and J. Goodenough, "Universal octahedral-site distortion in orthorhombic perovskite oxides," *Phys Rev Lett*, vol. 94, no. 6, p. 065501, 2005.

[67] G. Barrera, J. Bruno, T. Barron, and N. Allan, "Negative thermal expansion," *J Phys Condens Matter*, vol. 17, no. 4, p. R217, 2005.

[68] A. W. Sleight, M. A. Thundathil, and J. S. Evans, "Negative thermal expansion materials," May 1996. US Patent 5,514,360.

[69] K. W. Chapman, P. J. Chupas, and C. J. Kepert, "Compositional dependence of negative thermal expansion in the Prussian Blue analogues $M^{II}Pt^{IV}(CN)_6$ (M= Mn, Fe, Co, Ni, Cu, Zn, Cd)," *J Am Chem Soc*, vol. 128, no. 21, pp. 7009–7014, 2006.

[70] J. M. Skelton, D. Tiana, S. C. Parker, A. Togo, I. Tanaka, and A. Walsh, "Influence of the exchange-correlation functional on the quasi-harmonic lattice dynamics of II-VI semiconductors," *J Chem Phys*, vol. 143, no. 6, pp. –, 2015.

[71] A. Togo, L. Chaput, I. Tanaka, and G. Hug, "First-principles phonon calculations of thermal expansion in $Ti_3SiC_2$, $Ti_3AlC_2$, and $Ti_3GeC_2$," *Phys Rev B*, vol. 81, p. 174301, May 2010.

[72] D. W. Green *et al.*, *Perry's Chemical Engineers' Handbook*, vol. 796. McGraw-hill New York, 2008.

[73] H. P. Beck and F. Kühn, "Studies on $ABX_6$ compounds. III. The $SnZrCl_6$ structure type," *Z Anorg Allg Chem*, vol. 621, no. 10, pp. 1655–1658, 1995.

[74] E. Zaitseva, S. Medvedev, and L. Aslanov, "Crystal and molecular structures of cesium phenylpentachloroantimonate $Cs[PhSbCl_5]$, potassium phenylpentabromoantimonate $K[PhSbBr_5]$, and cesium hexachloroantimonate $Cs[SbCl_6]$," *J Struct Chem*, vol. 31, no. 1, pp. 92–97, 1990.

[75] A. Mar and J. A. Ibers, "The layered ternary germanium tellurides $zrgete_4$, $hfgete_4$, and $tigete_6$: structure, bonding, and physical properties," *J Am Chem Soc*, vol. 115, no. 8, pp. 3227–3238, 1993.

[76] W. Eichler and H.-J. Seifert, "Strukturelle und magnetische Untersuchungen an Hexachlorowolframaten(V)," *Z Anorg Allg Chem*, vol. 431, no. 1, pp. 123–133, 1977.

[77] I. Chung, J. Do, C. G. Canlas, D. P. Weliky, and M. G. Kanatzidis, "$APSe_6$ (A = K, Rb, and Cs): Polymeric selenophosphates with reversible phase—change properties," *Inorg Chem*, vol. 43, no. 9, pp. 2762–2764, 2004. PMID: 15106958.

[78] A. Ider, M. E. Farissi, and J. Laval, "Cationic ordering in tysonite type structures I: crystal structure of $BaTeF_6$," *J Fluor Chem*, vol. 99, no. 2, pp. 161 – 166, 1999.